Geophysical Research Letters

RESEARCH LETTER
10.1002/2018GL077051

Key Points:
- Vegetation "greening" and soil "drying" cooccurs over 42% of global vegetated land in a large GCM ensemble
- The greening and drying pattern is driven by changes in precipitation partitioning at the land surface
- These results highlight an intrinsic future trade-off between terrestrial vegetation (green water) versus total runoff (blue water)

Supporting Information:
- Supporting Information S1
- Figure S1
- Figure S2
- Figure S3
- Figure S4
- Text S1

Correspondence to:
J. S. Mankin,
mankin@dartmouth.edu

Citation:
Mankin, J. S., Seager, R., Smerdon, J. E., Cook, B. I., Williams, A. P., & Horton, R. M. (2018). Blue water trade-offs with vegetation in a CO_2-enriched climate. *Geophysical Research Letters*, *45*, 3115–3125. https://doi.org/10.1002/2018GL077051

Received 5 JAN 2018
Accepted 15 MAR 2018
Accepted article online 23 MAR 2018
Published online 6 APR 2018

Blue Water Trade-Offs With Vegetation in a CO_2-Enriched Climate

Justin S. Mankin[1,2,3], Richard Seager[1], Jason E. Smerdon[1], Benjamin I. Cook[1,3], A. Park Williams[1], and Radley M. Horton[1,3]

[1]Lamont-Doherty Earth Observatory of Columbia University, Palisades, NY, USA, [2]Department of Geography, Dartmouth College, Hanover, NH, USA, [3]NASA Goddard Institute for Space Studies, New York, NY, USA

Abstract Present and future freshwater availability and drought risks are physically tied to the responses of surface vegetation to increasing CO_2. A single-model large ensemble identifies the occurrence of colocated warming- and CO_2-induced leaf area index increases with summer soil moisture declines. This pattern of "greening" and "drying," which occurs over 42% of global vegetated land area, is largely attributable to changes in the partitioning of precipitation at the land surface away from runoff and toward terrestrial vegetation ecosystems. Changes in runoff and ecosystem partitioning are inversely related, with changes in runoff partitioning being governed by changes in precipitation (mean and extremes) and ecosystem partitioning being governed by ecosystem water use and surface resistance to evapotranspiration (ET). Projections show that warming-influenced and CO_2-enriched terrestrial vegetation ecosystems use water that historically would have been partitioned to runoff over 48% of global vegetated land areas, largely in Western North America, the Amazon, and Europe, many of the same regions with colocated greening and drying. These results have implications for how water available for people will change in response to anthropogenic warming and raise important questions about model representations of vegetation water responses to high CO_2.

Plain Language Summary Using a large ensemble of simulations from a state-of-the-art Earth System Model, we show that 42% of global vegetated land areas are projected to have "greening" in the form of additional vegetation growth at the same time as "drying" in the form of reduced soil moisture in a business-as-usual world. Simultaneous greening and drying is curious and suggests that future ecosystems—which could demand more water due to warmer and longer growing seasons and CO_2 fertilization—siphon water that historically would have become the runoff that fills rivers and streams, termed "blue water." We show that warming and changes in plant growth from CO_2 creates an explicit water trade-off in which future vegetation directly diminishes runoff relatively or absolutely for nearly half of global land areas. Our results have important implications for future water availability, but also point to the crucial importance of resolving model uncertainties associated with terrestrial vegetation and its response to increasing CO_2.

1. Introduction

Global warming will affect the terrestrial water cycle with vegetation playing a key role in mediating changes between the atmospheric and land surface branches of the hydrological cycle. However, the net effects of vegetation on future surface water availability in streams and soils, which are of key interest to people, are challenging to hypothesize given the myriad responses and feedbacks that plants induce (e.g., Arneth et al., 2010; Betts et al., 2004; Field et al., 2007). Accurately quantifying the net effects is nevertheless critical, because vegetation could serve to ameliorate or aggravate the tendency toward surface drying due to atmospheric warming projected by aridity metrics (cf. Ault et al., 2016; Cook et al., 2014; Greve et al., 2017; Milly & Dunne, 2016; Roderick et al., 2015; Scheff & Frierson, 2015; Scheff et al., 2017; Sherwood & Fu, 2014; Swann et al., 2016).

Direct plant physiological responses to elevated CO_2 concentrations such as stomatal closure could lessen (Idso & Brazel, 1984; Milly & Dunne, 2016; Roderick et al., 2015; Swann et al., 2016) or enhance (Betts et al., 2004; Skinner et al., 2017) land surface drying. Stomatal closure increases surface resistance

to evapotranspiration (ET) that, all else being equal, would increase runoff and soil moisture (Idso & Brazel, 1984; Milly & Dunne, 2016; Roderick et al., 2015; Swann et al., 2016). Increased plant water use efficiency (WUE) from higher atmospheric carbon could also create a wetting effect (Swann et al., 2016), as vegetation could fix the same amount of carbon while transpiring less water, regardless of stomatal responses. But these effects—that in isolation might contribute to increased runoff—also drive feedbacks that can aggravate atmospheric warming and surface drying. Stomatal closure from high CO_2, for example, is also a physiological forcing on climate, enhancing sensible heat fluxes (Betts et al., 2004) and hence, plausibly, warm season heat waves (Skinner et al., 2017). Additional plant growth from CO_2-stimulated photosynthesis (CO_2 fertilization) and warming effects, also shares this duality of ameliorating and aggravating soil drying and runoff declines (Mankin, Smerdon, et al., 2017): increased vegetation/leaf areas can enhance latent heat fluxes, terrestrial water recycling, evaporative cooling, and precipitation; but it can also increase ecosystem water demands, drawing down the runoff and soil moisture formerly available in the warm season. This projected drying is linked to the increased ecosystem water demands from both radiatively driven warming and additional plant growth ("greening") that outpace the ET decreases from stomatal resistance increases. Such a response of simultaneous "greening" and "drying" in terms of increasing leaf areas coupled with declining soil moisture and runoff, is projected in parts of the American West (e.g., Mankin, Smerdon, et al., 2017), has some observational basis (e.g., Frank et al., 2015; Ukkola et al., 2016), and suggests the possibility that radiatively- and biogeochemically -driven increases in ecosystem water demands could increase the proportion of water that terrestrial vegetation siphons from streamflow, with consequences for riverine ecosystems and people.

To investigate these issues, we analyze a large single-model ensemble of climate projections to provide the first assessment of the global extent of colocated greening and drying in climate projections and the associated implications for runoff (herein referred to as "blue water"; see, for example, World Water Assessment Programme, 2009). Our effort centers on identifying where CO_2- and warming-induced vegetation growth takes up water that, in a historical climate, would have gone to blue water. We characterize this response by developing a simple metric called Blue Water Trade-off (BWT) that quantifies the change in how precipitation is partitioned to vegetation and blue water at the land surface. Our analysis addresses the following questions: (1) Where does colocated summer greening and drying occur? (2) What physically accounts for this pattern of greening and drying? and (3) What does greening and drying imply for changes in blue water?

2. Data and Methods

2.1. Climate Model Data

Climate model data come from the fully coupled National Center for Atmospheric Research Community Earth System Model (NCAR CESM-LE or LENS), which is an ensemble experiment designed to give a robust estimate of the forced climate response relative to the influence of internal climate variability (see Kay et al., 2015 for details). Here we use 35 simulations from the LENS historical (1920–2005) and 21st century simulations (2006–2100) in a high-emissions pathway (RCP8.5) (Kay et al., 2015; Meinshausen et al., 2011). LENS uses minor differences in the atmospheric initial conditions for each ensemble member to provide an estimate of CESM's representation of internal variability (Kay et al., 2015; Mankin et al., 2015; Mankin, Smerdon, et al., 2017; Mankin, Viviroli, et al., 2017).

We use the following monthly-scale gridded hydroclimatic quantities from the ensemble: precipitation (sum of "SNOW" and "RAIN," mm/s), canopy evaporation ("QVEGE," mm/s), transpiration ("QVEGT," mm/s), soil evaporation ("QSOIL," mm/s), volumetric soil moisture (from the hydrologically active top 10 levels (0–~3 m) of soil, "H2OSOI," m^3/m^3), total runoff ("QRUNOFF," mm/s), leaf area index ('TLAI,' unitless), canopy temperature ("Tv," K), 2 m relative humidity ("RH2M," %), and net primary productivity ("NPP," gC m^{-2} s^{-1}). We also analyze daily scale precipitation (mm/s).

2.2. Analysis

For each individual ensemble member and grid point, we analyze climatological average water year (WY) totals, which we define here as the sum between September and August in the Northern Hemisphere and March and February in the Southern Hemisphere, so that the end of the WY coincides with the end of the summer season (see Mankin, Smerdon, et al., 2017). For variables presented as summer averages, they are defined as boreal (June–August) and austral (December–February) standards. The historical climatology is taken as the mean of the end of the historical simulation (1976–2005), while the end-of-century interval is the mean of 2071–2100.

Following Mankin, Smerdon, et al. (2017), we calculate both the canopy water flux as the sum of transpiration and canopy evaporation and vegetation WUE as the ratio between average net primary productivity (NPP, $gC \cdot m^{-2} \cdot s^{-1}$) and annual average transpiration; largely similar results are derived from a calculation of WUE using gross primary productivity, GPP, as shown in the supporting information. Canopy vapor pressure deficit ("VPD," kPA) is calculated as the difference between the actual vapor pressure and the saturation vapor pressure at the canopy temperature. Extreme precipitation is calculated based on the 5-day precipitation extremes (known as "PX5D"), conventionally defined as the annual maximum precipitation total in any successive period of 5 days. We calculate canopy conductance to ET (G_s) using the relation in CESM's land model, which formulates the bulk canopy water fluxes (C) as a function of the canopy vapor pressure deficit (VPD, defined above) as $G_s = \frac{1}{R_s} = \frac{C}{\mathrm{VPD}}$, where R_s is the sum of leaf boundary layer and stomatal resistances (Oleson et al., 2010). All percentages in figures and text are reported as a percent of "global vegetated land area," which is defined as the total land area with less than 50% bare soil at the end of the 21st century. Ensemble mean significance is tested using a Student's t test at the 5% level against the variability of the 35 ensemble members. All maps presenting ensemble mean changes only color grid points with significant changes; the grid point is not colored if it is not significant.

To estimate precipitation partitioning at the land surface and its change with forcing, we use a simple budget. Climatological total water year (WY) precipitation (P) at the grid point scale can be approximated by the sum of the WY total bulk canopy water flux (transpiration plus leaf evaporation, C), WY total surface and subsurface runoff (Q, 'blue water'), and a WY term encapsulating all other possibilities of precipitation partitioning such as direct soil evaporation, aquifer, and soil recharge, and multiyear snow and canopy storage that we call WY soil + storage (S):

$$P = C + Q + S \tag{1}$$

where all variables are climatological WY totals and are in units of mm (see end-of-century change in Figure S1). Precipitation partitioning ratios presented in all figures are calculated as follows: canopy partitioning is the ratio of the WY canopy water flux to WY precipitation (C/P); partitioning to blue water runoff (Q/P), and soil+storage (S/P), are calculated similarly.

2.3. Derivation of Blue Water Trade-Off

To quantify the explicit water trade-off among vegetation and surface and subsurface runoff (blue water), we develop a metric called the Blue Water Trade-off (BWT) as follows: Based on the budget presented in equation (1), the precipitation that is partitioned to the canopy and blue water can be written as

$$\varphi = P - S = C + Q \tag{2}$$

The climatological change in the amount of WY precipitation that is shared solely among the canopy and blue water between two time periods, f and h, is represented as

$$\Delta\varphi = \left[P_f - S_f\right] - \left[P_h - S_h\right] = \left[C_f + Q_f\right] - \left[C_h + Q_h\right] \tag{3}$$

We emphasize that this precipitation amount is calculated as a function of S, which changes only modestly relative to the other terms (Figure S1c). If the partitioning ratio of precipitation among C and Q is stationary between f and h, then we can predict the expected change in the WY total canopy water flux ($\widehat{\Delta C}$, where the $\hat{\cdot}$ denotes prediction) using β_c, which is the historical ratio of C to φ:

$$\beta_c = \frac{C_h}{\varphi_h} \tag{4}$$

$$\widehat{\Delta C} = \beta_c \cdot \Delta\varphi \tag{5}$$

Similarly for blue water,

$$\beta_q = \frac{Q_h}{\varphi_h} \tag{6}$$

$$\widehat{\Delta Q} = \beta_q \cdot \Delta\varphi \tag{7}$$

The historical partitioning ratios (β_q and β_c) are not stationary in the actual model simulations—they evolve with forcing. Because $\Delta\varphi$ is the precipitation that must be partitioned among Q and C and because $\beta_q + \beta_c = 1$, we can isolate the amount of blue water lost to terrestrial vegetation, or vice versa, based on the model-projected change in precipitation partitioning among the two. Thus, the difference between the predicted change in the canopy water flux ($\widehat{\Delta C}$) based on a stationary partitioning ratio and its actual change in the LENS (ΔC) is given by

$$E_c = \Delta C - \widehat{\Delta C} \tag{8}$$

If $E_c > 0$, then ecosystems are gaining water at the expense of blue water. If $E_c < 0$ then blue water increases at the expense of ecosystems. Note also that as defined, if both $P - S$ and $C + Q$ change, but the partitioning ratio among C and Q remains the same, then $E_c = 0$. E_c is what we present herein as the BWT metric. Positive values of BWT represent the amount of precipitation going to terrestrial vegetation ecosystems that would have otherwise gone to blue water runoff under historical or stationary partitioning; it is vice versa for negative values.

3. Results

3.1. Where Does Colocated Summer Greening and Drying Occur?

The end-of-the-century global WY precipitation response from LENS is statistically significant and positive over 78% of global vegetated land area (Figure 1a). This response is consistent in both pattern and magnitude with the median annual-scale response of the CMIP5 ensemble: (1) significant increases over middle and high latitudes (of ~5–10%) and the tropics, save for parts of the Amazon, the North American Southwest, the Mediterranean, South Africa, and Southwestern Australia, and (2) decreases that are either significant or uncertain in the subtropics (e.g., Figure AI.SM8.5.9 from van Oldenborgh et al., 2013 and Pendergrass et al., 2015).

Despite widespread WY precipitation increases over the middle and high latitudes, summer soil moisture does not reflect this spatial pattern of centennial-scale wetting (Figure1b). The summer soil moisture response integrated over the hydrologically active layers (0–3 m) instead shows statistically significant reductions over ~46% of global vegetated land area, encompassing vast portions of North and South America and most of continental Europe; many of these regions are colocated with WY precipitation increases. Collectively, some 34% of global vegetated land area displays this pattern of increased precipitation coinciding with seasonal soil drying (Figure 1c). These regions are contrasted with vast regions of significant summer soil wetting: ~46% of vegetated land area has colocated increases in summer soil moisture and WY precipitation (seen in the Southeastern U.S., the Pantanal and Pampas in South America, the Congo and the southern reaches of the African Sahel, as well as Asia, Siberia, and most of the Australian continent).

Although there are regional differences in combined precipitation and soil moisture trends, leaf area index (LAI) trends are generally positive, with 88% of global vegetated land area showing significant summer increases (unhatched regions in Figure 1b)—an indication of large-scale carbon assimilation by surface vegetation due to both the radiative (longer and warmer growing seasons) and fertilization (amplified photosynthesis) effects of CO_2 (e.g., Figures S2a and S2b). Notably, these LAI increases are nearly as likely to be in regions with seasonal soil moisture declines (42% of global vegetated land area) as they are with soil moisture increases (45% of global vegetated land area; Figure 1b).

3.2. What Physically Accounts for Projected Greening and Drying?

To identify the causes of colocated greening and drying, we formalize the associated relationships among changes in precipitation, LAI, soil moisture, and bulk water fluxes in Figures 1c–1f. There is generally a positive association among the changes in summer soil moisture and WY precipitation, and this is also associated with increases in LAI (Figure 1c). Importantly, ~33% of vegetated land areas have decreasing soil moisture at the same time as increasing precipitation and LAI. Furthermore, increasing VPD from warming is strongly related to increasing bulk canopy water flux, highlighting the crucial role that warming plays in elevating atmospheric and ecosystem water demands, though also to increasing LAI, indicating that physiological changes can allow this to cooccur with greening (Figure S2b).

Because the spatial pattern of soil moisture decline is more heterogeneous than LAI changes (e.g., see red hatching in Figure 1b denoting the few areas of summer LAI decreases), we examine the factors associated with surface drying. Figure 1d highlights that changes in the soil + storage term [S in equation (1)]

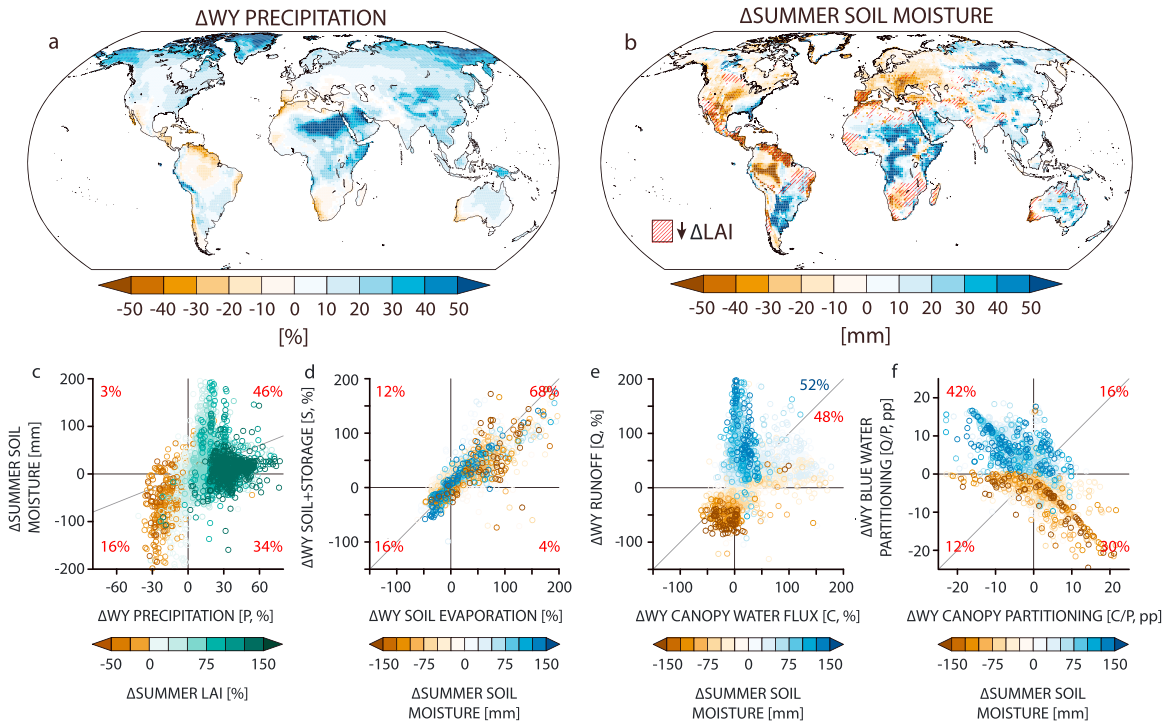

Figure 1. Ensemble mean change (2071–2100 minus 1976–2005) in (a) total water year (WY) precipitation (%) and (b) 0–3 m summer soil moisture (mm) and leaf area index (LAI) change. Colors indicate the statistically significant change. In (b), red hatching covers the regions where summer LAI decreases or has insignificant change, everywhere else LAI significantly increases. (c) End-of-century ensemble mean grid point change in WY precipitation (%) versus the change in summer soil moisture (mm). Colors represent the change in summer LAI (%). (d) Change in WY soil evaporation (%) versus the change in WY S (%). (e) Change in WY C (%) versus the change in WY Q (%). (f) Change in the canopy partitioning (C/P, percentage points, pp) versus the change in WY runoff partitioning (Q/P, pp). Colors in (d)–(f) represent the change in summer soil moisture (mm). Red text in (c), (d), and (f) reports the percentage of global vegetated land area falling in each quadrant. Blue (red) text in (e) indicates the percentage of vegetated land area above (below) the 1:1 line.

are largely determined by changes in soil evaporation but that changes in soil + storage do not strongly relate to—and therefore, likely do not account for—soil moisture drying (Figures S1, S4a, and S4c). Changes in the WY bulk canopy water flux, blue water, and summer soil moisture do not show a strong association (Figure 1e), but the direction of soil moisture changes appear to be more directly related to runoff changes or whether bulk canopy flux changes increase more than blue water fluxes: points falling above the 1:1 line in Figure 1e tend to be associated with soil moisture increases while those below the line tend to be associated with soil moisture declines. Locations with the deepest soil moisture drying are associated with runoff declines that are more negative than canopy water flux declines.

While changes in the bulk water fluxes to runoff or the canopy generally reflect the direction of soil moisture change (Figure 1e), a number of places do not follow this relationship. If we instead examine the change in the precipitation partitioning ratio to canopies (herein canopy partitioning, C/P) and to runoff (herein blue water partitioning, Q/P), the relationship among the directions of change in soil moisture, the canopy water flux, and blue water are clarified (Figure 1f). The change in the partitioning of precipitation between the canopy water flux and blue water (C/P versus Q/P) shows a strong inverse relationship, with increased partitioning to the canopy being associated with reduced partitioning to blue water. Notable is a strong shift of soil moisture change from positive to negative as blue water partitioning becomes negative (Figure 1f). Thus, while the bulk water fluxes from the canopy and blue water are weakly positively correlated (Figure 1e), changes in their partitioning ratios are inversely related and more strongly so (Figure 1f). Furthermore, drier summer soils tend to be associated with an increased fraction of WY precipitation going to the canopy, a decreased fraction going to runoff, and increased WY soil evaporation.

Given the strong relationships among soil moisture and the precipitation partitioning ratios shown in Figure 1f, we examine the spatial pattern of precipitation partitioning at the surface to identify whether it

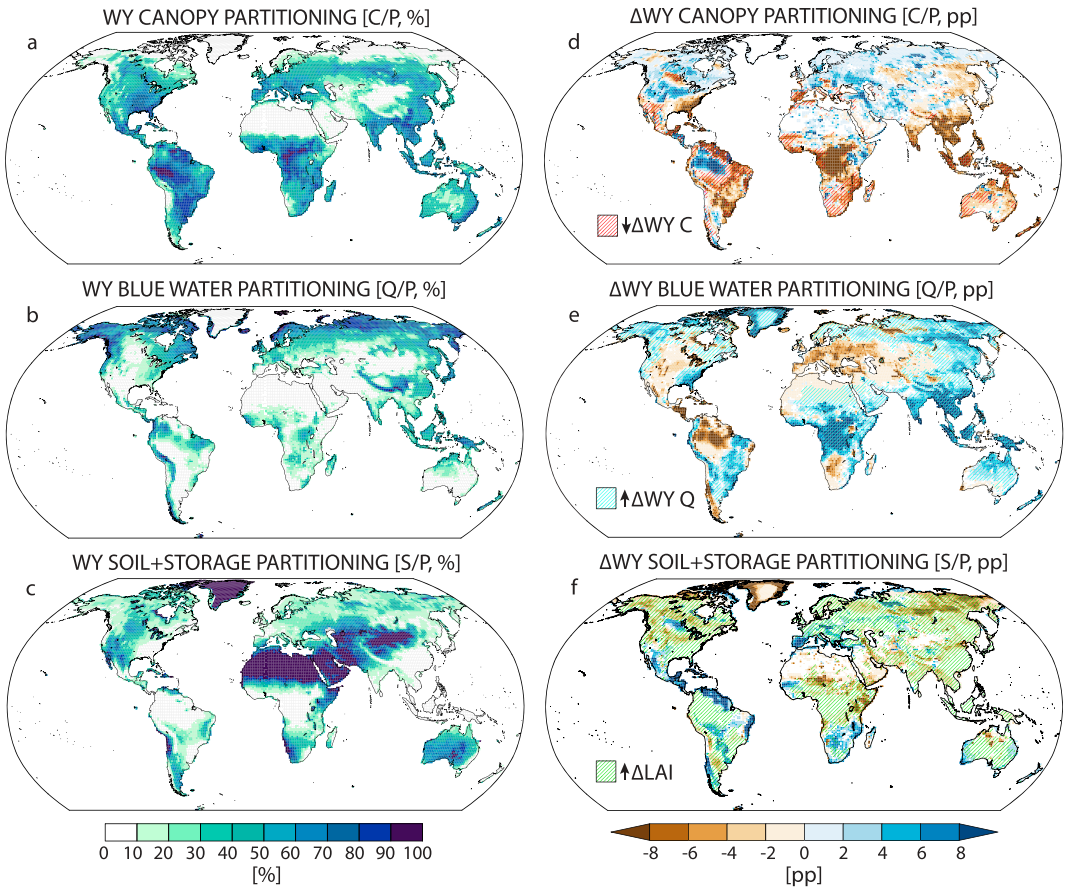

Figure 2. Historical (1979–2005) ensemble mean WY precipitation partitioning to (a) the canopy (C/P), (b) blue water (Q/P), and (c) soil + storage (S/P), all in percent (%). Ensemble mean changes (2071–2100 minus 1976–2005) in percentage points (pp) of (d) canopy, (e) blue water, and (f) soil + storage partitioning. In (d)–(f), colors show the statistically significant change. In (d), red hatching covers regions where WY canopy water fluxes decrease or do not significantly change. In (e), turquoise hatching covers regions where WY blue water runoff significantly increases. In (f), green hatching covers regions of significant LAI increases.

clarifies the cause of the greening and drying seen in Figure 1b. Figure 2 presents the historical WY precipitation partitioning to the canopy (C/P), blue water runoff (Q/P), and soil + storage (S/P) as well as their end-of-century changes. The historical climatologies make clear that for the majority of densely vegetated regions, such as the Southeastern U.S., the Amazon and Congo basins, and South and Southeast Asia, the dominant pathway for precipitation is to return to the atmosphere via transpiration and canopy evaporation. Blue water partitioning is the dominant pathway in the high latitudes and mountainous regions, where energy limitations restrict evaporation and frozen soils and/or low-vegetation water demands generate runoff (Figure 2b), consistent with predictions from the Budyko framework (Budyko, 1974). Alternative pathways (represented by soil+storage partitioning) dominate precipitation partitioning over water-limited regions (Figures 2c and S4c).

Figures 2d–2f illustrate the end-of-the-century change for precipitation partitioning. Where vegetation consumes an increased fraction of total WY precipitation—such as the Amazon basin, northern and central Rocky Mountains and northern Great Plains of North America, and parts of the Mediterranean, continental Europe, and the Middle East—blue water partitioning tends to decrease (cf. Figures 2d and 2e), as does absolute runoff (Figure S1b). Not all regions adhere to this one-for-one pattern: high-latitude Siberia and North America as well as much of East Africa and the Pampas region of Argentina exhibit increases in both canopy and blue water partitioning (Figures 2d and 2e)—a function of the decreased soil + storage partitioning in those regions (Figure 2f). Globally, the majority of vegetated land areas have an increase in blue water partitioning (59%) while about 41% see an increase in canopy partitioning.

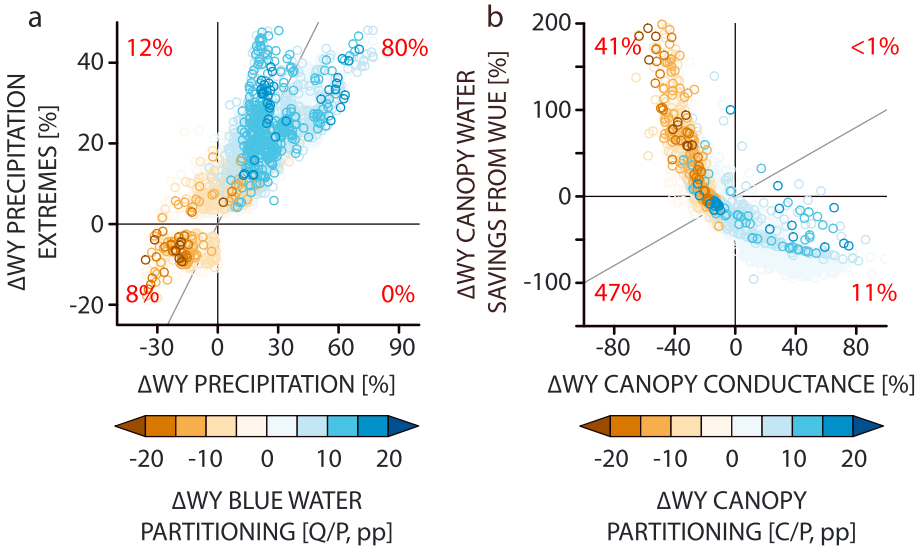

Figure 3. Drivers of precipitation partitioning changes, showing the (a) change in the WY precipitation (P, %) versus the change in WY 5-day precipitation extremes (PX5D, %). Colors represent the change in WY blue water partitioning ($\Delta(Q/P)$, pp). (b) The change in the WY canopy conductance (ΔG_s, %) versus the change in the WY canopy water savings from WUE changes, calculated as the change in the ratio of WUE to LAI [$\Delta(WUE/LAI)$, %]. Colors represent the change in WY canopy partitioning [$\Delta(C/P)$, pp]. In each, we show the 1:1 line. Red text reports the percentage of global vegetated land area falling in each quadrant.

The canopy water flux (C) increases over the majority of land areas, encompassing some 59% of the globe (Figures 2d and S1a). However, it also decreases in portions of southwest North America and Central America, Caribbean South America and the Brazilian Cerrado, as well as the Iberian Peninsula, southwestern Africa, Indonesia, and western Australia. The hatched areas in Figure 2e show that WY runoff significantly increases over ~61% of total global land area. Those regions with decreased blue water partitioning tend to be associated with net decreases in WY runoff as well, (lack of hatching in those regions in Figure 2e). Absolute changes in soil + storage are small relative to canopy and blue water fluxes (Figure S1). Furthermore, because our focus is on greening and drying and there are no clear spatial relationships between soil moisture declines (drying), widespread LAI increases (greening), and soil + storage partitioning (cf. Figures 1b, 1d, and 2f), we do not focus further on soil + storage partitioning.

We identify the drivers of the partitioning changes to canopies and blue water in Figure 3 for all vegetated land points globally, highlighting the coherence of the relationships despite the high degree of spatial heterogeneity in greening and drying. In CESM, runoff is simulated using the SIMTOP scheme, where surface runoff is parameterized as infiltration excess, while baseflow is a product of a simple decay function applied to the theoretical maximum baseflow (Niu et al., 2005; Oleson et al., 2010). The sum of surface and subsurface flow (the blue water runoff we analyze) is then routed to a separate River Transport Model (RTM) within CESM (Oleson et al., 2010). In steady state, runoff at the surface and subsurface in SIMTOP is balanced by precipitation minus evapotranspiration (Niu et al., 2005). Because of this control, we examine changes in both the mean and tails of the precipitation distribution and how that influences blue water partitioning (Figure 3a). Increases in mean precipitation tend to increase blue water partitioning, as soil saturation (inducing baseflow) and infiltration excess (inducing surface runoff) increase. An increase in precipitation intensity is associated with positive blue water partitioning, denoted by the linear relationship among mean precipitation, 5-day precipitation extremes, and the sign change in runoff partitioning changes (Figure 3a). Increased precipitation intensity would diminish canopy interception and increase saturation excess runoff, thus increasing blue water partitioning.

In contrast to blue water partitioning, canopy partitioning is governed by a more complex set of processes. In the land component of CESM, bulk canopy water fluxes are a function of warming-driven changes in VPD and the total leaf- and boundary-level resistances to ET. Ecosystem-level partitioning also is influenced by net ecosystem water demand and how that water demand changes as a function of changes in WUE and LAI from both warming and CO_2 effects. We therefore present all of these terms in Figure 3b, showing the association

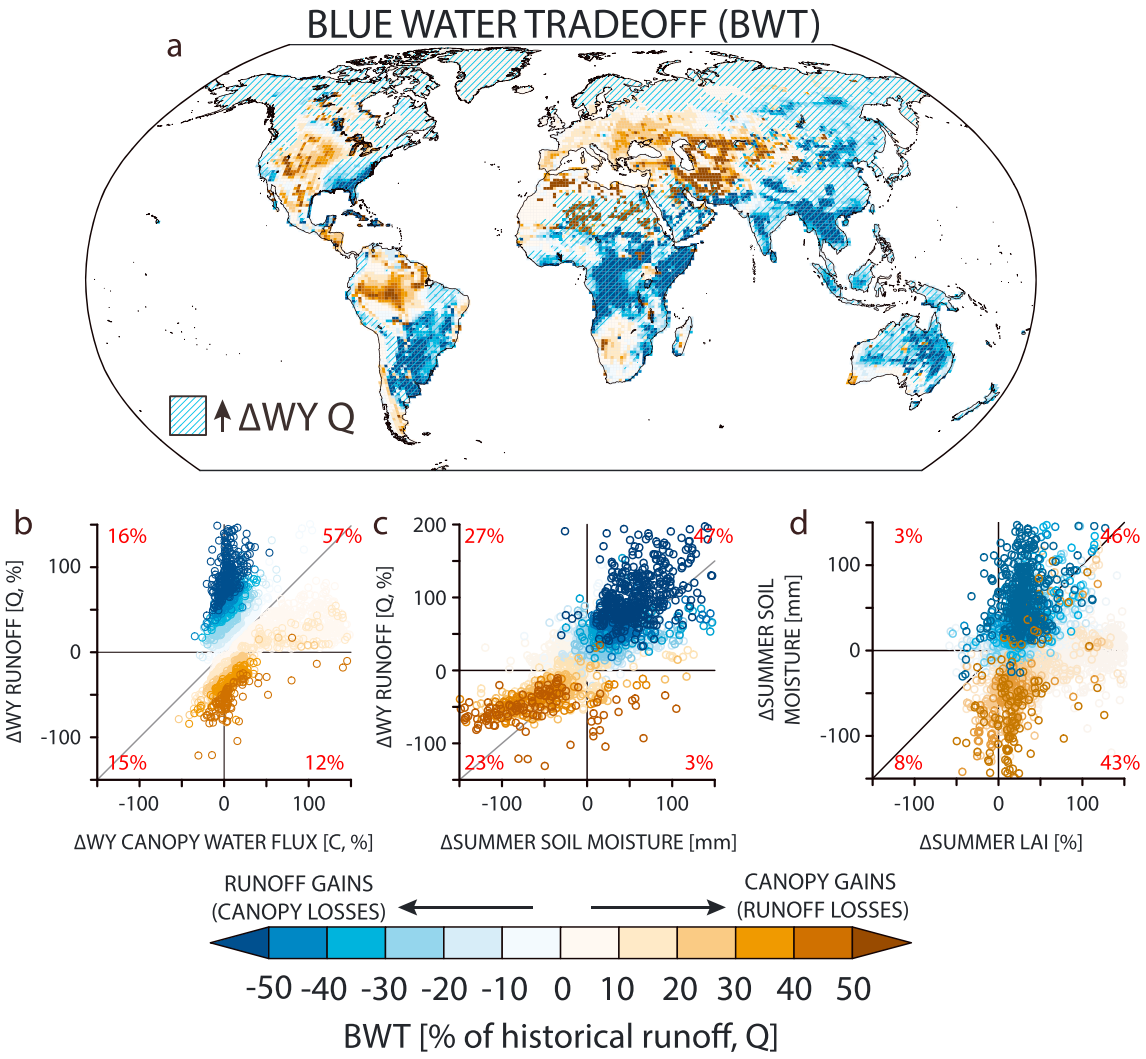

Figure 4. Blue water trade-off (BWT). (a) End-of-the-century BWT expressed as a percentage of historical (1979–2005) blue water runoff (Q, %). (b) As in Figure 1e, end-of-century change in the WY canopy water flux (C, %) versus that for WY blue water runoff (Q, %). (c) End-of-century change in summer soil moisture (mm) versus that for WY blue water runoff (Q, %). (d) End-of-century change in summer LAI versus that for summer soil moisture. In all panels blue colors (negative values) indicate the increased amount of precipitation partitioned to blue water runoff and away from the terrestrial vegetation, while brown colors (positive values) indicate the increased amount of precipitation partitioning to vegetation and away from blue water runoff. In (b)–(d), red text reports the percentage of global vegetated land area falling in each quadrant.

among statistically significant changes in canopy conductance (G_s) to ET plotted against the canopy water savings from WUE changes. The latter is calculated as the change in the ratio of WUE to LAI (Δ(WUE/LAI), %), and is a measure of whether increases in WUE are outpaced by additional water demands from increased vegetation growth. We note that the Δ(WUE/LAI) ratio is constructed in native units, and as such, only serves as an indication of whether WUE changes are relatively larger or smaller than LAI changes. Clearly as WUE gains outpace LAI gains (positive *y* axis), the canopy uses a decreasing fraction of precipitation, denoted by the brown colors in the second quadrant of Figure 3b. In contrast, as additional vegetation growth and evaporative demand outpaces WUE gains (Δ(WUE/LAI) < 0) and canopy conductance increases ($\Delta G_s > 0$), the canopy partitioning increases. Thus, while soil moisture, runoff, and the canopy water flux all share a weak positive association, when water is being stressed or limited (either through increased evaporative demands, LAI increases that outpace WUE gains, and/or decreased mean WY precipitation) the canopy water flux tends to increase as a fraction of precipitation.

3.3. What Do Projected Changes in Precipitation Partitioning Imply for Changes in Blue Water?

To formalize the trade-off that occurs between future ecosystems and blue water and to quantify the water availability consequences of greening and drying, we present the BWT metric in Figure 4 (see section 2

for definition; we also present the metric in mm in Figure S3). The metric quantifies the amount of water gained by ecosystems or lost to blue water relative to a world in which precipitation changes occur as projected, but its partitioning remains stationary. Positive brown values in Figure 4 indicate canopy gains, as less water flows to blue water and instead flows to the canopy, while negative (blue) values indicate runoff gains, as less water flows to the canopy and instead flows to blue water. Approximately 48% of the global vegetated land area exhibits positive values, representing precipitation that is siphoned from blue water by warming- and CO_2-induced vegetation growth (canopy gains). Most of the North American continent, the Amazon basin, continental Europe and the Middle East have positive BWT values, as vegetation takes water from runoff. In contrast, 52% of the global land area has negative BWT values, representing increased runoff partitioning away from vegetation. Large-magnitude BWT losses are visible in the southeastern U.S., Atlantic coast of South America, the Congo basin, and East Africa, as well as the Subcontinent and Asia, as water is reallocated from vegetation to runoff.

Figure 4b presents how the BWT values show a clear separation of increases and decreases of bulk canopy flux (C) and blue water runoff (Q) along the 1:1 line. Such separation emphasizes that the largest runoff gains are associated with modest changes in the canopy water flux. Reductions in blue water similarly occur in regions where increases in the canopy water flux are larger than those for runoff or decreases in the canopy water flux are less negative than those for runoff. This metric itself provides additional evidence for the relationships in Figures 1e and 1f—summer drying in the soil column is nearly always associated with changes in canopy water fluxes that are larger (or less negative) than those for blue water, or an increased canopy partitioning as vegetation takes water from runoff and dries out the soil column. Confirmation of this is provided in Figure 4c, where positive BWT (canopy gains) clearly map to decreases in both absolute summer soil moisture and WY runoff. Thus, despite being a metric based on changes in relative partitioning, BWT changes do account for the drying in the soil column and net decreases in runoff, while the soil + storage (S) term does not (Figures S4b and S4c). In Figure 4d, we return to the greening and drying pattern that motivated our inquiry and show its relationship with the BWT metric. Approximately 75% of the vegetated land area with both increased LAI and decreased soil moisture exhibits positive values of BWT, highlighting the clear association of cooccurring greening and drying and water availability changes, as future terrestrial vegetation ecosystems siphon water directly to the sacrifice of blue water runoff.

4. Discussion and Conclusions

Greening and drying cooccur in over 40% of the global vegetated land area by the end of the century under a high-emissions scenario in LENS, encompassing much of North America, the Amazon basin, and continental Europe (Figure 1b). Such a response can even occur in locations exhibiting net increases in WY precipitation, such as North America and parts of Europe (Figures 1a and 1c). Because canopies tend to increase everywhere driven by CO_2- and warming-induced carbon assimilation by vegetation (Figures 1b and S2a and S2b), the spatial variation in the greening and drying phenomenon is driven primarily by spatial variation in drying. Such drying is a function of changes in land surface partitioning of precipitation between either blue water runoff or the canopy (Figures 1d–1f and 2). The processes governing changes in precipitation partitioning are linked to the model physics: increased blue water partitioning occurs primarily due to mean increases in precipitation that are reinforced by an increase in precipitation extremes (Figure 3a), while increased canopy partitioning occurs due to a combination of radiative warming and increases in LAI and canopy conductance that outpace gains in WUE (Figures 3b and S2c). Such increased relative or absolute canopy water demands are likely driven by a combination of warmer and longer growing seasons (Figure S2b), increased precipitation (Figure 1a), and CO_2 fertilization effects (Figure 3b). Together, the net effects of these processes on precipitation partitioning account for water gains and losses to and from the canopy and runoff, which we explicitly quantify against a world in which such partitioning does not change (BWT shown in Figures 4, S3, and S4). The BWT metric developed herein indicates where canopy water gains come directly at the sacrifice of runoff gains and vice versa. The metric also clarifies the water availability implications of projected greening and drying by quantifying the percent of historical runoff lost or gained due to changing vegetation water demands driven by both radiative and biogeochemical effects (Figure 4d).

Our results indicate that regions projected to both green and dry during the summer do so because of radiative and biogeochemical effects on vegetation water demands from increased warming and direct CO_2 effects, like fertilization. Such changes, however, are subject to numerous poorly constrained responses of plants to both warming and CO_2. Nonetheless, they suggest that there is a potential trade-off between blue water

availability and water needs of terrestrial vegetation arising from ecosystem responses to warming and CO_2, despite anticipated increases in stomatal resistance that could increase surface moisture. This picture is partially complicated by human productive use of ET (such as in areas of rainfed agriculture), which could benefit in our framework. The benefit of the BWT metric is nevertheless that it quantifies changes in surface water availability in terms of changing terrestrial vegetation water demands due to radiative and biogeochemical changes. At the same time, however, it points to the larger set of model assumptions that underpin how precipitation partitioning is altered by vegetation responses to the radiative and physiological effects of CO_2. To this point we have taken the response of the CESM as plausible—that colocated greening and drying is a potential real-world climate response arising from anthropogenic emissions. Earth System Models (ESMs), such as CESM, have nevertheless increased their biogeochemical, biogeophysical, and physiological sophistication in representing land surface processes (e.g., Clark et al. (2015)) and there has been little systematic evaluation of how model representations of the soil-plant-atmosphere continuum and its response under high CO_2 influence assessments of drought or aridity changes (Mankin, Smerdon, et al., 2017). Canopy density increases, plant structural acclimation, carbon allocation, nutrient limitations, rooting depths, soil water stress, and respiration changes, in addition to the interactions with underrepresented hillslope hydrology and other effects, will influence ecosystem water demands under radiative forcing and warming, beyond the expected surface resistance increases to ET. It is thus critical to assess how vegetation is simulated in ESMs, separating radiative from physiological effects and their consequent influences in order to understand the physics of projected drying, the origins and consequences of biases in projected drying, and their implications for predictions of future water availability for people and ecosystems over the near and long term.

Acknowledgments
We acknowledge the CESM1 (CAM5) Large Ensemble Community Project generated by the National Center for Atmospheric Research (NCAR) and Naomi Henderson and Haibo Liu for the data serving and computing support in the Division of Ocean and Climate Physics at Lamont-Doherty Earth Observatory of Columbia University. Our work was supported by the Earth Institute, the Vetlesen Foundation, and the Center for Climate and Life, the NASA Modeling, Analysis, and Prediction program (MAP) and NASA 80NSSC17K0265, and U.S. National Science Foundation grants AGS-1703029, AGS-1243204, and AGS-1401400. This is Lamont contribution number 8201.

References

Arneth, A., Harrison, S. P., Zaehle, S., Tsigaridis, K., Menon, S., Bartlein, P. J., et al. (2010). Terrestrial biogeochemical feedbacks in the climate system. *Nature Geoscience*, *3*(8), 525–532. https://doi.org/10.1038/ngeo905

Ault, T. R., Mankin, J. S., Cook, B. I., & Smerdon, J. E. (2016). Relative impacts of mitigation, temperature, and precipitation on 21st-century megadrought risk in the American Southwest. *Science Advances*, 1–9. https://doi.org/10.1126/sciadv.1600873

Betts, R. A., Cox, P. M., Collins, M., Harris, P. P., Huntingford, C., & Jones, C. D. (2004). The role of ecosystem-atmosphere interactions in simulated Amazonian precipitation decrease and forest dieback under global climate warming. *Theoretical and Applied Climatology*, *78*(1–3), 157–175. https://doi.org/10.1007/s00704-004-0050-y

Budyko, M. I. (1974). VI climatic factors of geographical zonality. *Geophysical Journal International*, *18*(C), 317–370. https://doi.org/10.1016/S0074-6142(09)60011-5

Clark, M. P., Fan, Y., Lawrence, D. M., Adam, J. C., Bolster, D., Gochis, D. J., et al. (2015). Improving the representation of hydrologic processes in Earth System Models. *Water Resources Research*, *51*, 5929—5956. https://doi.org/10.1002/2015WR017096

Cook, B. I., Smerdon, J. E., Seager, R., & Coats, S. (2014). Global warming and 21st century drying. *Climate Dynamics*, 2607–2627. https://doi.org/10.1007/s00382-014-2075-y

Field, C. B., Lobell, D. B., Peters, H. A., & Chiariello, N. R. (2007). Feedbacks of terrestrial ecosystems to climate change. *Annual Review of Environment and Resources*, *32*(1), 1–29. https://doi.org/10.1146/annurev.energy.32. 053006.141119

Frank, D. C., Poulter, B., Saurer, M., Esper, J., Huntingford, C., Helle, G., et al. (2015). Water-use efficiency and transpiration across European forests during the Anthropocene. *Nature Climate Change*, *5*(6), 579–583. https://doi.org/10.1038/nclimate2614

Greve, P., Roderick, M. L., & Seneviratne, S. I. (2017). Simulated changes in aridity from the last glacial. *Environmental Research Letters*, *12*(114021).

Idso, S. B., & Brazel, A. J. (1984). Rising atmospheric carbon dioxide concentrations may increase streamflow. *Nature*, *312*(5989), 51–53. https://doi.org/10.1038/312051a0

Kay, J. E., Deser, C., Phillips, A., Mai, A., Hannay, C., Strand, G., et al. (2015). The Community Earth System Model (CESM) large ensemble project: A community resource for studying climate change in the presence of internal climate variability. *Bulletin of the American Meteorological Society*, *96*(8), 1333–1349. https://doi.org/10.1175/BAMS-D-13-00255.1

Mankin, J. S., Smerdon, J. E., Cook, B. I., Williams, A. P., & Seager, R. (2017). The curious case of projected 21st-century drying but greening in the American West. *Journal of Climate*, *30*(21), 8689–8710. https://doi.org/10.1175/JCLI-D-17-0213.1

Mankin, J. S., Viviroli, D., Mekonnen, M. M., Hoekstra, A. Y., Horton, R. M., Smerdon, J. E., & Diffenbaugh, N. S. (2017). Influence of internal variability on population exposure to hydroclimatic changes. *Environmental Research Letters*, *12*(4), 044007. https://doi.org/10.1088/1748-9326/aa5efc

Mankin, J. S., Viviroli, D., Singh, D., Hoekstra, A. Y., & Diffenbaugh, N. S. (2015). The potential for snow to supply human water demand in the present and future. *Environmental Research Letters*, *10*(11), 114016. https://doi.org/10.1088/1748-9326/10/11/114016

Meinshausen, M., Smith, S. J., Calvin, K., Daniel, J. S., Kainuma, M., Lamarque, J.-F., et al. (2011). The RCP greenhouse gas concentrations and their extensions from 1765 to 2300. *Climatic Change*, *109*(1-2), 213–241. https://doi.org/10.1007/s10584-011-0156-z

Milly, P. C. D., & Dunne, K. A. (2016). Potential evapotranspiration and continental drying. *Nature Climate Change*, *6*, 946–949. https://doi.org/10.1038/NCLIMATE3046

Niu, G. Y., Yang, Z. L., Dickinson, R. E., & Gulden, L. E. (2005). A simple TOPMODEL-based runoff parameterization (SIMTOP) for use in global climate models. *Journal of Geophysical Research*, *110*, D21106. https://doi.org/10.1029/2005JD006111

Oleson, K. W., Lawrence, D. M., Gordon, B., Flanner, M. G., Kluzek, E., Peter, J., et al. (2010). Technical description of version 4.0 of the Community Land Model (CLM) (Tech. Rep. April). National Center for Atmospheric Research. https://doi.org/10.5065/D6RR1W7M

Pendergrass, A. G., Lehner, F., Sanderson, B. M., & Xu, Y. (2015). Does extreme precipitation intensity depend on the emissions scenario? *Geophysical Research Letters*, *42*, 8767–8774. https://doi.org/10.1002/2015GL065854

Roderick, M. L., Greve, P., & Farquhar, G. D. (2015). On the assessment of aridity with changes in atmospheric CO_2. *Water Resources Research*, *51*, 5450–5463. https://doi.org/10.1002/2015WR017031

Scheff, J., & Frierson, D. M. W. (2015). Terrestrial aridity and its response to greenhouse warming across CMIP5 climate models. *Journal of Climate*, *28*(14), 5583–5600. https://doi.org/10.1175/JCLI-D-14-00480.1

Scheff, J., Seager, R., Liu, H., Coats, S., Scheff, J., Seager, R., et al. (2017). Are glacials dry? Consequences for paleoclimatology and for greenhouse warming. *Journal of Climate*, *30*, 6593–6609. https://doi.org/10.1175/JCLI-D-16-0854.1

Sherwood, S., & Fu, Q. (2014). A drier future?. *Science*, *343*(6172), 737–739. https://doi.org/10.1126/science.1247620

Skinner, C. B., Poulsen, C. J., Chadwick, R., Diffenbaugh, N. S., Fiorella, R. P., Skinner, C. B., et al. (2017). The role of plant CO_2 physiological forcing in shaping future daily-scale precipitation. *Journal of Climate*, *30*(7), 2319–2340. https://doi.org/10.1175/JCLI-D-16-0603.1

Swann, A. L. S., Hoffman, F. M., Koven, C. D., & Randerson, J. T. (2016). Plant responses to increasing CO_2 reduce estimates of climate impacts on drought severity. *Proceedings of the National Academy of Sciences of the United States of America*, *113*(36), 10,019–10,024. https://doi.org/10.1073/pnas.1604581113

Ukkola, A. M., Prentice, I. C., Keenan, T. F., Van Dijk, A. I., Viney, N. R., Myneni, R. B., & Bi, J. (2016). Reduced streamflow in water-stressed climates consistent with CO_2 effects on vegetation. *Nature Climate Change*, *6*(1), 75–78. https://doi.org/10.1038/nclimate2831

van Oldenborgh, G. J., Collins, M., Arblaster, J. M., Christensen, J. H., Marotzke, J., Power, S. B., et al. (2013). Annex I: Atlas of global and regional climate projections. *Intergovernmental Panel on Climate Change*, 1–159.

World Water Assessment Programme (2009). *The United Nations World Water Development Report 3: Water in a changing world* (p. 349). Paris, London: UNESCO, Earthscan. https://doi.org/10.3390/w3020618